The Influence of Repeated Heat Treatments on The Propagation of Fatigue Cracking of Medium Carburized Steel

Majid Khaleel Najem, Jamal Nayief Sultan
Northern technical university/ Tech. Eng. College-Power Mech. Eng. Dep., - Mosul, IRAQ

Emad Toma Karash[*]*, Adel M. Ali, Hssein A. Ibrhim*
Northern Technical University - Technical Institute Mosul, IRAQ
[*]*emadbane2007@ntu.edu.iq*

ABSTRACT

The issue of metal fatigue emerged as one of the major issues in a variety of engineering designs, and the design engineers were forced to take metals' fatigue resistance into account. In this paper, multiple quenching mediums and varied heat treatments were utilized to examine the effects of various heat treatments on the development of fatigue cracking in steel. The model that was carburized, quenched in distilled water and tempered before being quenched once more in distilled water and tempered a second time had the best outcomes, the fewest cycles needed to cause the model to fail, and a correlation between the rate of fatigue crack propagation and the length of the crack, according to the results. Additionally, the analytical findings demonstrated that this model, as opposed to models with fixed stress intensity factors, has a fatigue crack growth rate. The model that was carburized, quenched in coolant, then tempered and quenched again without performing the tempered appearance failed very rapidly. The high rate of the stress intensity factor with fatigue crack propagation is shown by the data analysis. The results show a reduction in the growth amount tendency of fatigue crack in the linear region mode-III.

Keywords: *Tensile Strength; Fatigue; Heat Treatment; Grain Structure; Quenching; Tempering, Carburized*

ISSN 1823-5514, eISSN 2550-164X

https://doi.org/10.24191/jmeche.v20i3.23920

Received for review: 2022-11-17
Accepted for publication: 2023-06-08
Published: 2023-09-15

Introduction

Engineering machinery and installations must fulfill the following three main requirements: to perform the required work, and function intended, have an appropriate and acceptable life service, and be able to perform production at reasonable costs. Appropriate operating period is taken into account in approximate ways at the design mode for parts subjected to repeated loads because most of the design engineers are not sufficiently familiar with the art of operation with time. Its parts after an inappropriate period of operation. The occurrence of this collapse is frequent with fatigue, so its importance increases with machines whose performance requires the presence of the property of light weight of the metal and thus the occurrence of high stresses in the metal during operation, and aircraft is one of the clear examples of this where light weight is of paramount importance.

Metal fatigue has received great attention to obtain adequate safety for machinery and engineering facilities, especially those whose collapse causes loss of life, as in the issues of aircraft parts design, where strict rules were imposed in the design so that those parts would have an appropriate resistance to fatigue. The main principles and comparisons are made based on experience to determine the acceptable fatigue resistance, as it is taken into account when designing that when a crack occurs, it does not have a destructive influence, and these rules determine the duration of operation of those different parts. In [1], they investigated the crack associated with macro-pitting in the gearbox bearing. They used the technique of accelerated bench top test to find the difference in performance between hardened AISI 52100 steel and carburized AISI 3310 steel. They found that the time of the appearance of pitting in the surface in AISI 3310 steel is twice that of hardened AISI 52100 steel.

Using the finite element method, the depth of the carburized case of SAE 8620 steel gears was predicted [2]. The martensitic growth in grain inside the carburized case, and by simulation, check the influence of carburizing and different adherent austenite contents on the large fatigue action of SAE 8620 steel catalytic gears. The model used shows that the depth of the case increases with growing heat treatment temperature and time. A large number of studies have shown that surface carburizing treatment can significantly improve the fatigue performance of steel [3]-[4]. Heat treatment techniques have been studied on stress in gears, as well as different cooling media and a mathematical and experimental model has been proposed [5]. The bending stress on carbon steel was studied and compared with the carbonization of conventional gas, and they concluded that the gas-carburized models have less resistance to all of the traditional gas-carburized models [6]. In this study [7], the relationship between the modality of how different cracks propagated and the microstructure of steel was studied. They found that decreasing the induction heat temperature from (1043-1143 K)

increases the crack propagation resistance by 30%. In [8], they investigated numerically and experimentally carburized AISI 8620 steels. They found that the results gated by numerical agreement with that got experimentally. While in [9], a mathematical model (elastic-plastic) was created using the finite element method, and this model relies on tests with the presence of a first slit to study the growth of fatigue cracking. The results showed that the hardness difference is linear from the outer surface of the model to the inside in the core of the model. In [10], the microstructure was studied on the growth of fatigue cracking of the carbonized models, and the results showed that the samples with a microstructure containing martensitic have better resistance to the growth of fatigue crack progression than those samples containing in the microstructure ferrite. Authors in [11] combined the scanning electron microscope images and Photoshop software, then the conversion rate between pixels and actual length of scale were calculated, after that the cracks parameters were known by pixel. A research in [12] provided a unified technique to evaluate changes in the amplitude of the microplasticity strain and intrinsic thermal dissipation for ASE 1045 steel. They discovered that the outcomes of this strategy are in excellent accord with those of the conventional method. In [13], they studied fatigue in the rolling contact performance of carburized steel and high-carbon steel, with the same volume fraction. The nanostructure Bainitic microstructures were obtained from the two alloy steels. They discovered that the carburized nanostructured bainitic steel's rolling contact fatigue life outperforms that of high-carbon steel. Then in [14], they studied the effect of adhesive austenite on rolling contact stress using stiffness tests, X-ray diffraction, scanning electron microscopy, and transmission electron microscopy. The rolling contact stress shows that the subsurface fragment life begins to increase as the adhesive austenite increases. The crack propagation rate of the carbon steel layer was evaluated according to SAE 4320, and it was found that as the carbon content decreased, the resistance to stress crack growth increased [15]. In [16], they used finite element modeling to find the influence of carbon allocation on residual stress in gears, then proposed a method to design the minimum case depth to obtain the lowest residual stresses. In [17], carburizing vacuum quenching and high-pressure gas were used for hollow rotational stress samples made with AISI 9310. The non-equilibrium shape has been shown to have little influence on the residual stress after quench solidification. While [18] used finite elements to thoroughly study the low-carbon steel carburization process. In [19], two allocation methods were used based on the prediction of crack characteristic size of Cr-Ni carbon steel alloy. The first is the generalized maximum and the second is the generalized Pareto allocation. The results show that the generalized maximum allocation can predict fatigue strength better than the generalized Pareto distribution allocation. In [20], a mathematical model was made to simulate a sliding gear, which is a hole for lubrication, and two models were used in that, and

the results showed that the samples with lead holes are more efficient in resisting fatigue cracking in the presence of contact stress. [21] This study focused on how austenitic grain size affected the onset and advancement of fatigue cracking for carbon steel's mode-II, and the results showed that the high leveling and finishing processes with the size of austenite grains led to an increase in the resistance to initiation and progression of fatigue cracking in the mode - II. Dynamic recrystallization was used to refine the grain size, as stated in [22]. The sliding dry wear behavior of martensite steel under various friction circumstances was taken into consideration by the authors of [23]-[24]. After being quenched and tempered twice, the microstructures and mechanical characteristics of steels with various carbon contents were examined [25]-[27]. The primary cause of this effect is the deformation of the original microstructures, which had an impact on how the microstructure changed during quenching and tempering [29]-[30]. This deformation led to the austenite grains becoming more refined and the carbides dissolving more quickly during the subsequent austenitization step [28]. With increasing initial hot rolling reduction, the results indicate an increase in Vickers hardness but a sizable drop in friction coefficient and wear rate [31].

In this article, different heat treatments, such as model quenching in different media, tempering, and repeated numerous times after carburizing on the models, are used to study the fatigue cracking propagation behavior of medium carbon steels. Selecting the most effective cooling method for usage following the quenching procedure and the kind of heat treatment. Additionally, specialized software will be employed to create equations that anticipate growth, development, and collapse under the impact of fatigue stresses.

Materials and Experimental Procedure

Materials

According to the German Standard, the medium carbon steel employed in this study is used in industry for a variety of purposes (DIN). A spectrometer was used to do a chemical analysis of the composition of medium carbon steels. Table 1 provides information on the metal used in the document's actual and typical chemical compositions.

Table 1: Results of chemical analysis for the metal used

Wt., %	C	Si	Mn	P	S	Mo	Cu	Fe
Standard value	0.42 - 0.5	0.15 - 0.35	0.5 - 0.8	≤ 0.035	≤ 0.035	-----	-----	Rem
Actual value	0.482	0.221	0.562	0.011	0.033	0.0788	0.0154	98.596

Carburization

After the extension of carburizing atoms to the surface of steel components, quenching and tempering at low temperatures is known as carburizing. The corrosion resistance, toughness, hardness, and other steel qualities can all be significantly enhanced through the carburizing process. After processing, the parts have a low-carbon martensite core that is strong and durable enough, and a hard, wear-resistant martensite surface with a small amount of soft carbide structure. We refer to steel that has been carbureted as having been carbureted. In this study, cylindrical carbon steel wear test samples were treated to a four-hour soaking time at 950 ℃ in a powder combination made up of 75% charcoal and 25% barium carbonate using pack carburizing techniques ($BaCO_3$). After the carburization procedure, the wear testing samples were split into three groups (A, B, and C) for heat treatment.

Heat treatments

The carburized steel specimens were split into three groups (A, B, and C) after heat treatment processes:

i. Group (A): All carburized steel samples were cooled to room temperature using a range of quenching media including solutions (distilled water, milk, motor oil, shampoo, water, sugar, cooling fluid, and food oil) after soaking for 20 minutes at a temperature of 780 ℃. The samples were then heated for 20 minutes at 230 °C.
ii. Group (B): Each piece of carburized steel was quenched in a different quenching fluid (distilled water, milk, motor oil, shampoo, water and sugar, cooling fluid, and food oil), after soaking for 20 minutes at 780 °C. Then, to temper the samples, they were all heated to 230 °C for 20 minutes. All previously quenched steel samples were once again quenched at 770 °C in distilled water.
iii. Group (C): All carburized steel samples were quenched in various quenching fluids (distilled water, milk, motor oil, shampoo, water and sugar, cooling fluid, and food oil), after soaking for 20 minutes at 780 °C. The samples were then heated to 230 °C and allowed to soak for 20 minutes. All previously quenched steel samples were then quenched a second time at 770 °C using distilled water as the quenching medium. Following that, each of the earlier steel samples was heated to (250 °C) for a twenty-minute soaking time.

Manufacture of fatigue test samples

The model's dimensions were as shown in Figure 1, and circular-section samples were employed with an initial incision that was 0.5 mm wide and 0.2 mm deep. The samples' ends were flattened at 90 ℃ to one another after being produced to the desired dimensions. To guarantee that the models' perimeters have an identical dimensional incision as shown in Figure 1. All samples that were used had their slit depth and sample diameter measured

using a coordinate measuring device. The stress ratio for all tests will be zero (R=0).

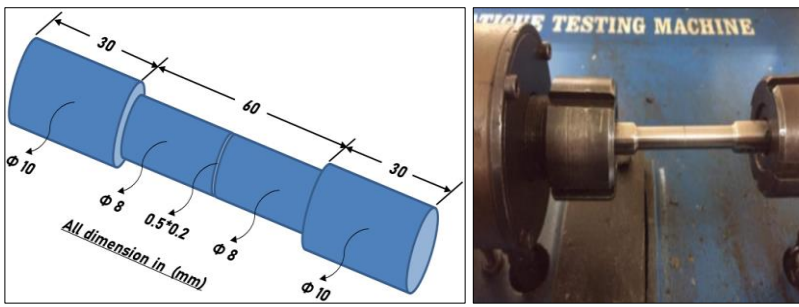

Figure 1: The machine and the dimensions of the model used in the test

Characterization of specimens from fatigue tests

To analyze the behavior of cracking propagation of the entire after executing various heat treatments, a 22 model of low-carbon steel was chosen (carburizing, quenching in different media, and tempering). They are categorized in Table 2.

Table 2: Classification of medium carbon steel samples used in fatigue tests

No.	Type of heat treatment	Group symbol - (A) (carbonation – quenching in different media, tempering)	Group symbol - (B) (carbonation – quenching in different media, tempering- quenching in distilled water)	Group symbol - (C) (carbonation – quenching in different media, tempering - quenching in distilled water, tempering)
1	At, receive		AS (As Received)	
2	Carbonation and quenching in shampoo	A 1	B 1	C 1
3	Carbonation and quenching in water &	A 2	B 2	C 2
4	Carbonation and quenching in milk	A 3	B 3	C 3
5	Carbonation and quenching in food oil	A 4	B 4	C 4
6	Carbonation and quenching in motor oil	A 5	B 5	C 5
7	Carbonation and quenching in cooling	A 6	B 6	C 6
8	Carbonation and quenching in distilled	A 7	B 7	C 7

Results and Discussion

Microstructure

The produced structures were studied using a Leica DM 2500 M microscope both before and after heat treatment.

Group A: (carbonation and quenching, tempering)

The microstructure of the first group samples (group A) is shown in Figure 2. These samples were quenched at 770 °C with a range of quenching solutions (distilled water, milk, motor oil, shampoo, water, sugar, cooling fluid, and food oil), before being tempered at 230 °C.

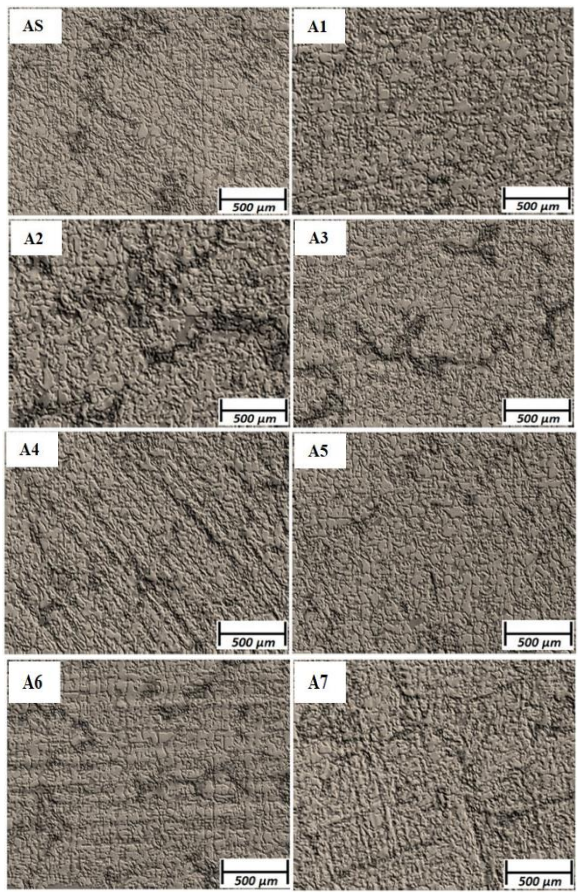

Figure 2: The microstructure of group a steel samples: carbonation – quenching, tempering

Group - B: (carbonation and quenching, tempering and quenching)

Figure 3 depicts the microstructure of the samples from the second group (group B). Carburized steel samples were quenched at 770 °C with a variety of quenching liquids (distilled water, milk, motor oil, shampoo, water, sugar, cooling fluid, and food oil), then heated to 230 °C temperature and quenched again at 770 °C using distilled water as a quenching liquid.

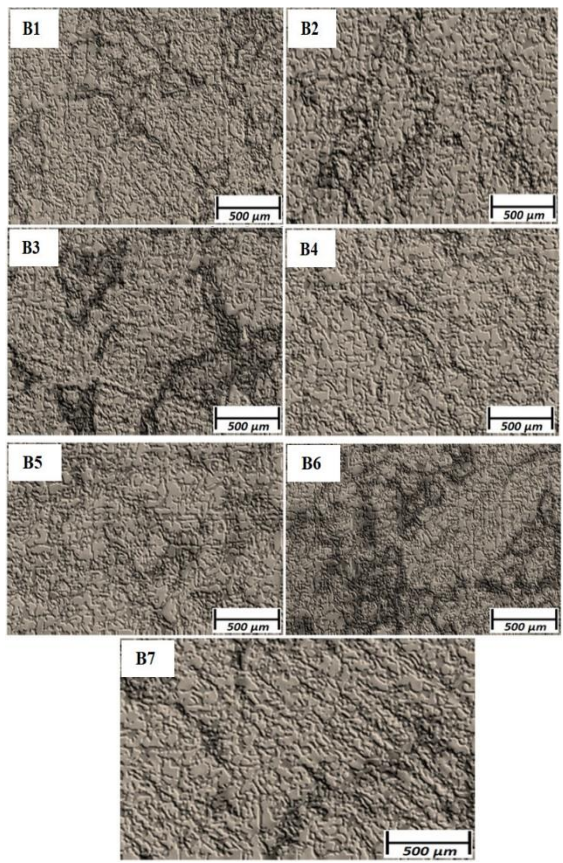

Figure 3: The microstructure of group (B) steel samples: carbonation – quenching, tempering- quenching

Group C: (carbonation, quenching, tempering and quenching, tempering)

Figure 4 depicts the microstructure of the samples from the third group (group C). In this group, several quenching liquids, such as food oil, milk, shampoo, motor oil, water with sugar, and cooling liquid, were used to

quench the carburized steel samples. They were then quenched once again with distilled water after being tempered at 230 °C. They underwent a second 250 °C tempering procedure after that.

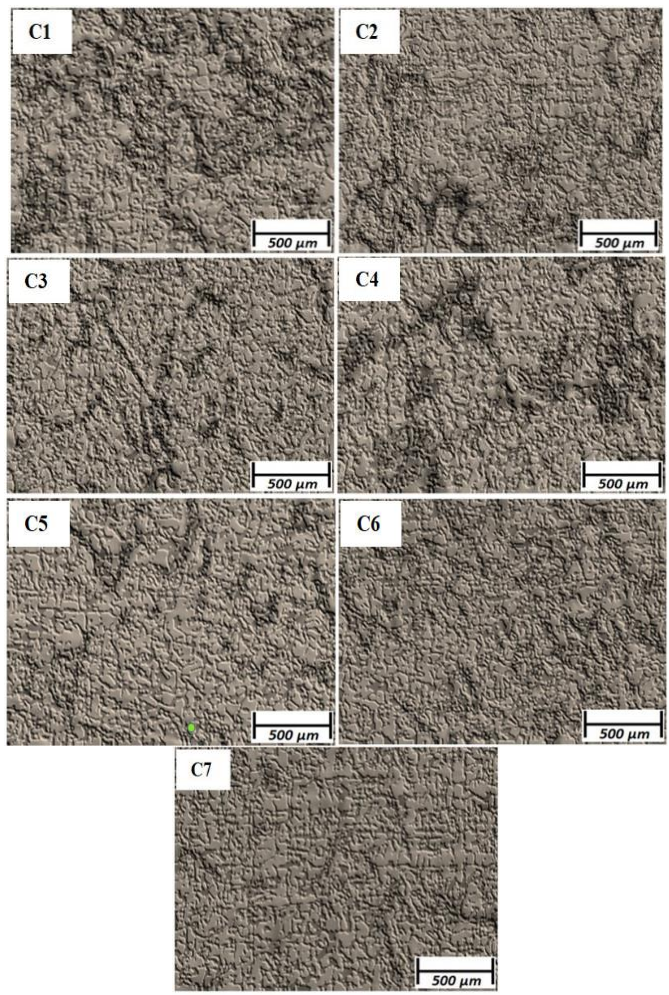

Figure 4: The microstructure of group (C) steel samples: carbonation – quenching, tempering - quenching, tempering

Figures 5-16 analyze the fatigue test results when a load of 171.073 MPa is applied to all samples that have undergone various heat treatments (distilled water, milk, motor oil, shampoo, water, sugar, cooling fluid, and food oil).

Schemes the length of the cycle number with the length of the crack

Figures 5-8 compare the findings for the three groups that were tested in terms of the association between the number of cycles and the crack length (A, B, and C). The cycle number and the crack duration for each model used in the test and in comparison to the original model are contrasted in Figure 5.

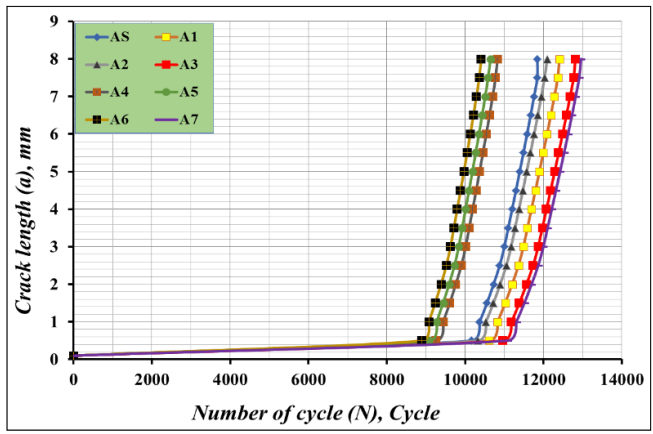

Figure 5: Appears group –A: the original specimen is compared to stress crack propagation curves

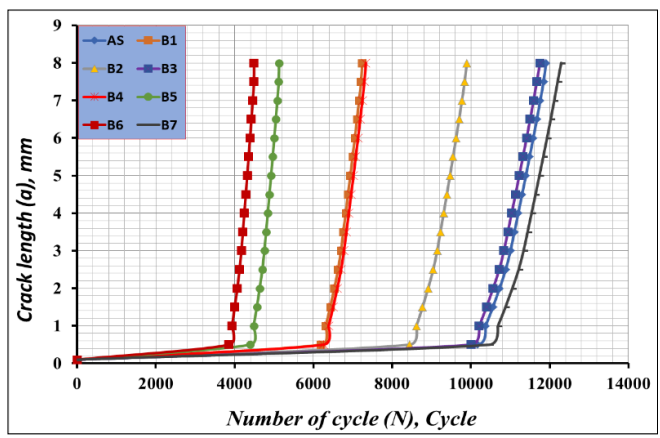

Figure 6: Appears group – B: The original specimen is compared to stress crack propagation curves

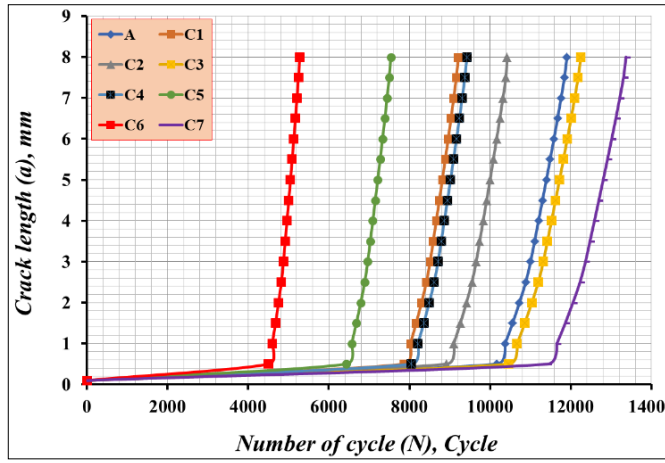

Figure 7: Appears group – C: The original specimen is compared to stress crack propagation curves

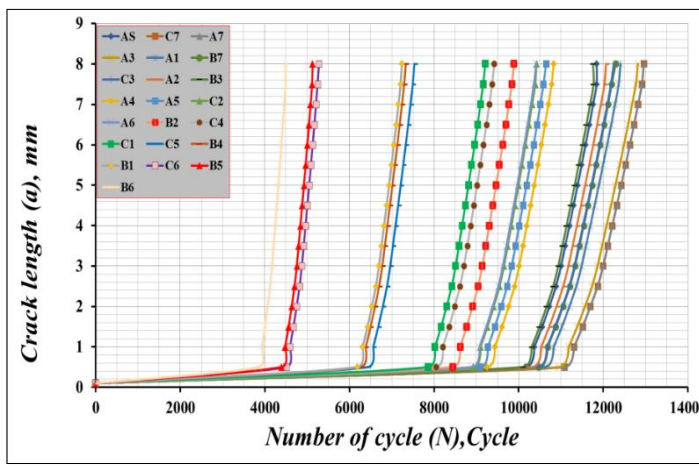

Figure 8: Appears all-groups: The original specimen is compared to stress crack propagation curves

Conclusion of the crack growth rate of fatigue

The crack growth rate (*da/dN*), and values of the fatigue were calculated using a finite difference (Newton forward difference, central finite difference, and Newton backward finite difference) method by entering all the values obtained from the various checks for the growth of the fatigue crack progression. For each of the analyzed models, Figures 9-12 display the

results of constructing those curves as well as the relationships between crack length (*a*) and crack development rate (*da/dN*).

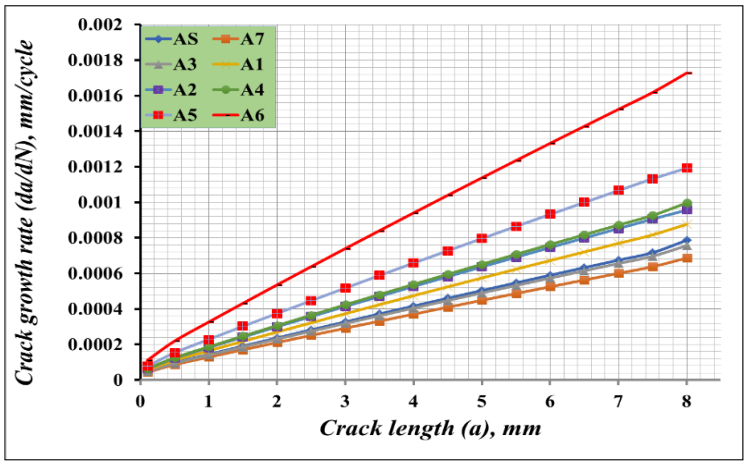

Figure 9: Shows the relation between fatigue crack growth rate and crack length for group A

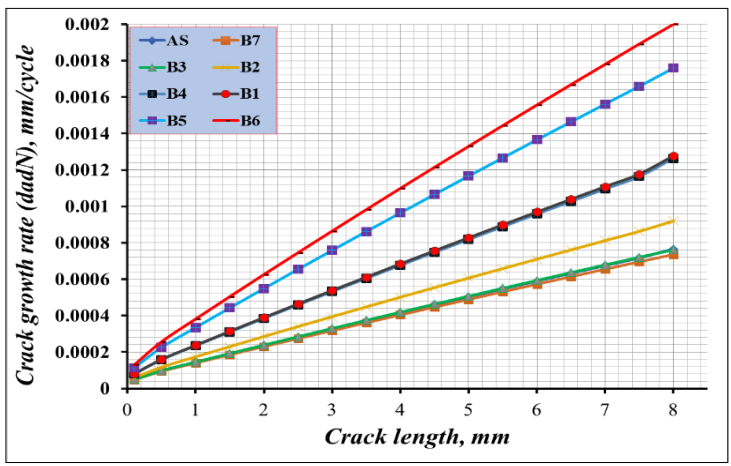

Figure 10: Demonstrates the connection between the length of group-B cracks and the rate of fatigue crack propagation.

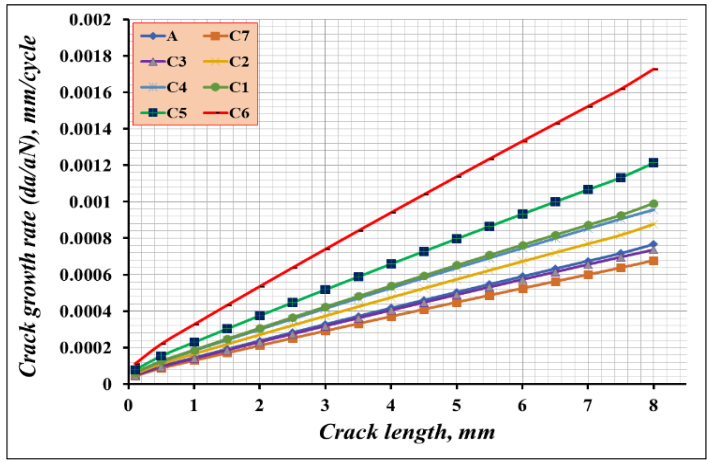

Figure 11: Demonstrates the connection between the length of the group-C crack and the rate of fatigue crack propagation

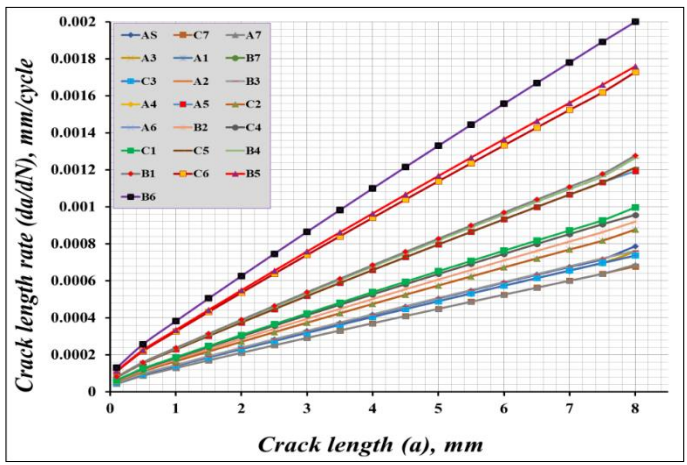

Figure 12: Demonstrates the connection between the length of cracks and the rate of fatigue crack propagation for all models

Measurement of fatigue crack propagation

For the models that had various heat treatments, 22 tests were conducted to ascertain the evolution of fatigue cracking with a first crack that had a depth of (0.2 mm), an extension of the fissure in a plane inclined at an angle of 45°, and the formation of a crack in the factory's roof. The evolution of fatigue cracking was measured using the direct current voltage drop method. By

referring to Figure 13 and using Equation (1), (2) and (3), the stress intensity factor (ΔK_{III}) was calculated [32].

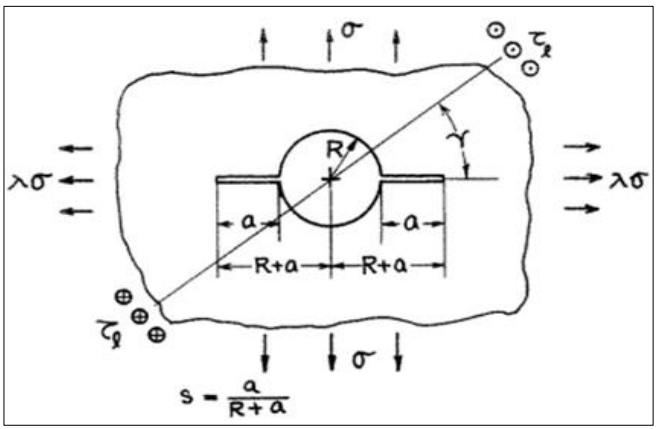

Figure 13: The model of fatigue crack propagation

$$\Delta K_{III} = \tau_N . \sqrt{\pi a} . F(s). \sin\gamma \quad (1)$$

where,

$$\tau_N = \frac{2\,T}{\pi\, a^3}; \quad (2)$$

$$F(s) = \sqrt{(2-s).(2-2s\&s^2)} \quad (3)$$

a= Crack length, *R*= Radius with slit of the specimen, *T*= Torque
τ_N= Net section shear stress

These criteria are given by Benthem and Koiter [33], and with accuracy is better than one percent, according to its exact method Asymptotic Approximation. A torque of *T*=175 Kg.cm=17167.5 N.mm was used and a first slit of *a*=0.2 mm was used, and the diameter of the shaft was *d*=8 mm. Figures 14-17 show the relation between the stress intensity factor (ΔK_{III}) and the fatigue cracking growth rate (*da/dN*) in the linear region mode - II, which is consistent with the Paris equation, and the mode – III which leads to the failure of the model, where the increased rate of fatigue cracking is fast in this area.

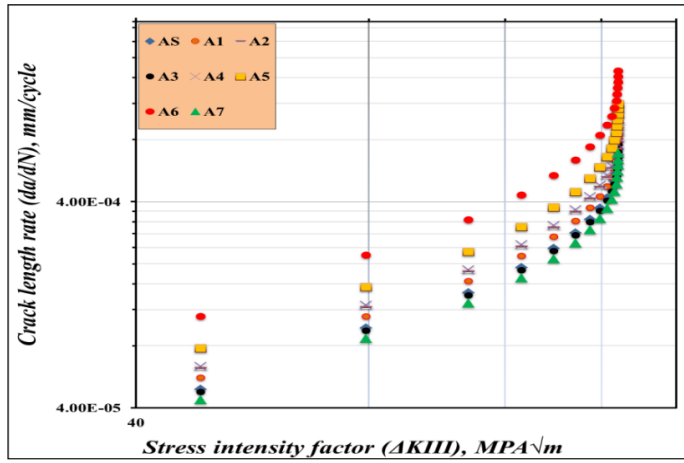

Figure 13: Relationship between the fatigue cracks growth rate (*da/dN*) and the factor of the stress concentration (K_{III}), at the linear region where the fatigue crack first appears, grows, and where the model breaks down for group-A

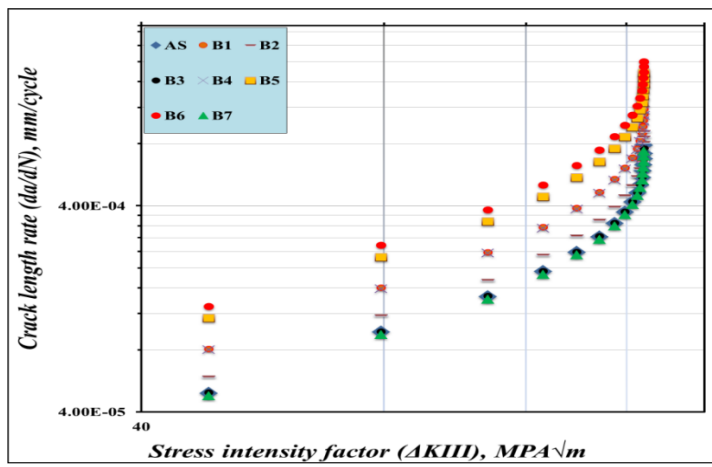

Figure 14: Relationship between the fatigue cracks growth rate (*da/dN*) and the factor of the stress concentration (K_{III}), at the linear region where the fatigue crack first appears, grows, and where the model breaks down for group-B

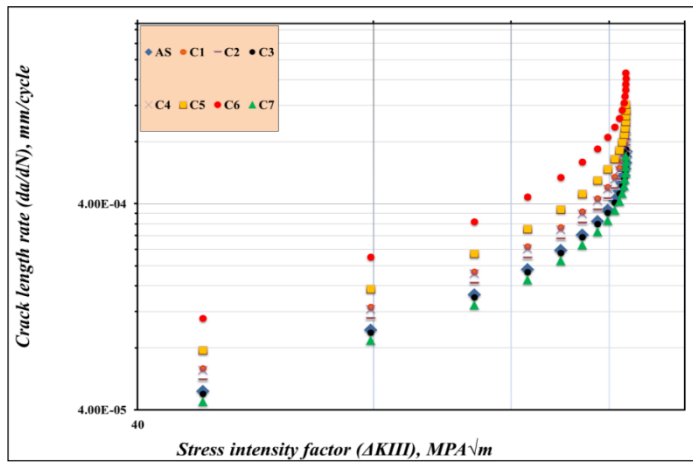

Figure 15: Relationship between the fatigue cracks growth rate (*da/dN*) and the factor of the stress concentration (K_{III}), at the linear region where the fatigue crack first appears, grows, and where the model breaks down for group-C

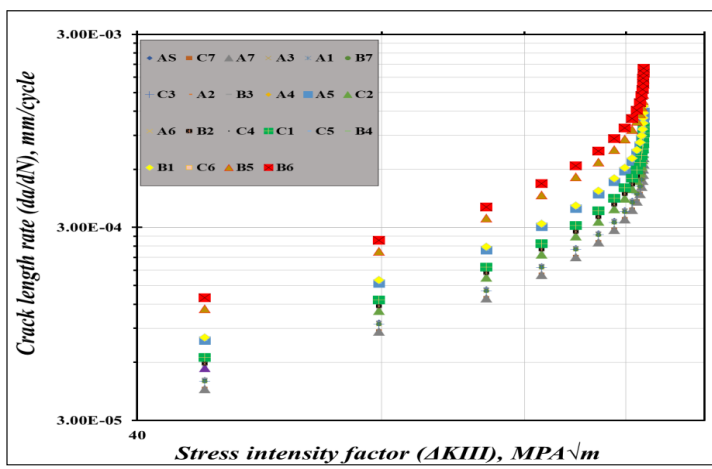

Figure 16: Relationship between the fatigue cracks growth rate (*da/dN*) and the factor of the stress concentration (K_{III}), at the linear region where the fatigue crack first appears, grows, and where the model breaks down for all specimens

The structure of martensitic resulting from the hardening of carbon steel in water hinders the growth of fatigue cracks. The fatigue limit rises as a

result of the interfacial barriers of the martensitic structure. The growth of these cracks is hindered by a larger microstructure consisting of martensite reviewed with a little bit of bainite, as this structure is characterized by being devoid of internal stresses that result from hardening, so the fatigue limit of the water-hardened steel increased.

Deduce crack growth behavior equations

For five models, including the original model, the best three models, and the worst model (AS, C7, A7, A3, and B6) to compare them, the Curve Expert program was used to derive the equations that describe the growth of the fatigue crack mode-III. Table 3 shows the values entered into the program, to obtain the fatigue cracks progress rate in the linear region. These equations are consistent with the Paris formula in the linear zone. The examination of those equations' findings is shown in the following Equations (4)-(8).

Table 3: It shows the values used to obtain the fatigue crack growth rate (Mode - III) in the linear region using the program Curve Expert

ΔK_{III}	AS (as received)	C7	A7	A3	B6
48.45533555	4.92028E-05	4.37833E-05	4.37833E-05	4.78285E-05	0.000129795
79.37775342	9.74173E-05	8.6687E-05	8.6687E-05	9.46962E-05	0.000256982
107.6715142	0.000144779	0.000128832	0.000128832	0.000140735	0.000381921
125.9996407	0.000191395	0.000170314	0.000170314	0.000186049	0.000504892
138.8219901	0.000237341	0.000211198	0.000211198	0.000230711	0.000626094
148.0347052	0.000282786	0.000251638	0.000251638	0.000274887	0.000745976
154.6795392	0.000327826	0.000291717	0.000291717	0.000318669	0.00086479
159.4244172	0.000372469	0.000331442	0.000331442	0.000362065	0.000982555
162.7409696	0.000416726	0.000370825	0.000370825	0.000405086	0.001099305
164.9839909	0.000460611	0.000409876	0.000409876	0.000447745	0.001215071
166.4314112	0.000504134	0.000448605	0.000448605	0.000490053	0.001329883
167.3058301	0.000547308	0.000487023	0.000487023	0.00053202	0.001443774
167.7864699	0.000590143	0.000525141	0.000525141	0.000573659	0.001556771
168.0157625	0.000632664	0.000562978	0.000562978	0.000614992	0.001668939
168.102807	0.000674885	0.000600548	0.000600548	0.000656034	0.001780315
171.2422576	0.000716884	0.000637951	0.000637951	0.00069685	0.001891599
168.1288912	0.000786884	0.000677951	0.000686884	0.000756884	0.001999654

$$\frac{da}{dN} = 2.245 * 10^{-6}\,\Delta K^{2.251} - 7.541 * 10^{-5}\,, \quad \text{for model (AS)} \qquad (4)$$

$$\frac{da}{dN} = 1.997 * 10^{-6}\,\Delta K^{2.011} - 6.711 * 10^{-5}, \quad \text{for model (C7)} \qquad (5)$$

$$\frac{da}{dN} = 1.997 * 10^{-6}\,\Delta K^{2.013} - 6.711 * 10^{-5}, \quad \text{for model (A7)} \qquad (6)$$

$$\frac{da}{dN} = 2.182 * 10^{-6}\,\Delta K^{2.125} - 7.331 * 10^{-5}, \quad \text{for model (A3)} \qquad (7)$$

$$\frac{da}{dN} = 5.922 * 10^{-6}\,\Delta K^{5.833} - 1.999 * 10^{-4}, \quad \text{for model (B6)} \qquad (8)$$

Conclusions

The following was discovered by comparing the results of the fatigue tests before and after the various heat treatments of carbonization and quenching in various mediums, as well as a tempering after quenching of all samples, and after evaluating the data in various programs:

i. The number of cycles required for the growth of the fatigue crack in the two models (A7, and C7) increased by 88.66% compared to the required cycles number in the original model (AS), while the number of cycles in the model (B6), which is the worst model in the tests, was less by 61.94% for the number of cycles in the original model (AS).
ii. The figures for the crack growth rate of fatigue show a noticeable fatigue crack growth rate increase in the worst model in the test, model B2, between $0\text{-}2*10^{-3}$, in comparison to the original model, whose value was between $0\text{-}0.69*10^{-3}$, and then the crack growth rate increase was in the two models (B5, and C6), where the values of the fatigue crack growth rate were between $0\text{-}1.88*10^{-3}$.
iii. The logarithmic figures demonstrate the relationship between the stress intensity factors and the crack length growth rate in the linear region mode - II. The model (B6) has a much higher crack length rate than the original model, but the variance in the two models' crack length rates is relatively small (A7, and C7). The figures also depict the failure zone of the model in the mode III region, where the fatigue rate values of the crack growth and the factor of stress intensity have converged. The crack development rate is rapid, and the failure process is swift in the mode III region.
iv. The obtained equations agree with the Paris formula for fatigue crack development growth and are shown by Curve Expert software with fatigue crack growth behavior in linear zone mode-III. Since the form has superior resistance to fatigue cracking, the tendency for crack progression in this area is reduced.

Contributions of Authors

The researchers emphasize and acknowledge equal contribution to each component of our effort. The final draft of this work has been reviewed and approved by all researchers.

Funding

There was no specific grant from any funding organization for this work.

Conflict of Interests

Our authors all certify that we have no conflicts interests.

Acknowledgment

The manuscript was funded by the Research Program of the Department of Mechanical Technology at the Northern Technical University-Technical Institute in Mosul, Iraq]. (No. 2021-00533).

References

[1] G. Benjamin, P. Mohanchand, G. D. Nicholaos, C. G. Aaron, R. S. Hyde, "The Impact of Steel Microstructure and Heat Treatment on the Formation of White Etching Cracks", *Journal of Tribology International*, vol. 134, pp. 232-239, 2019. https://doi.org/10.1016/j.triboint.2019.02.003.

[2] C. Edward, C. B. Henry, K. Y Hemantha, "Multi-length scale modeling of carburization, martensitic microstructure evolution and fatigue properties of steel gears", *Journal of Materials Science & Technology*, vol. 49, pp. 157-165, 2020. https://doi.org/10.1016/j.jmst.2019.10.044.

[3] N. Xiao, W. J. Hui, Y. J. Zhang, X. L. Zhao, Y. Chen, H. Dong, "High cycle fatigue behavior of a low carbon alloy steel: The influence of vacuum carburizing treatment", *Engineering Failure Analysis*, vol. 109, pp. 1-25, 2019. https://doi.org/10.1016/j.engfailanal.2019.104215.

[4] X. Yanjun, Y. Yongming, Y. Wenchao, D. Mingzhen, S. Jie, W. Maoqiu, "Microstructure and fatigue properties of 17Cr2Ni2MoVNb gear steel after gas carburizing and low-pressure carburizing",

International Journal of Fatigue, vol. 167, part A, p. 107314, 2023. https://doi.org/ 10.1016/j.ijfatigue.2022.107314.

[5] Y. Enesi, O. O. Salawu, A. Ajayi, A.P.I P. Inegbenebor, U.O. Uyor, "Effects of Heat Treatment Techniques on the Fatigue Behaviour of Steel Gears: A Review", *Journal of Physics: Conference Series*, vol. 1378, no 4, pp. 1-6, 2019. https://doi.org/10.1088/1742-6596/1378/4/042001.

[6] A. Osman, Ç. C. Ahmet, P. James, , B. Mohammed, "The influence of high temperature gas carburizing on bending fatigue strength of SAE 8620 steel", *Journal Materials & Design*, vol. 30, no. 5, pp. 1792-1797, 2009. https://doi.org/10.1016/j.surfcoat.2006.11.006.

[7] Kazuaki, Okada, O. Koji, T. Yoshikazu, A. Nozomu, "Crack propagation behavior of impact crack in case hardening steel subjected to combined heat treatment with excess vacuum carburizing and subsequent induction hardening", *International journal of Transactions of the Iron and Steel institute of Japan*, vol. 60, pp. 2576-2585, 2020. https://doi.org/ 10.2355/isijinternational.ISIJINT-2019-826.

[8] S. Yi, M. M. Sina, S. Farshid, P. Kristin, W.Trice, "Influence of engaged austenite Compressive residual stresses on rolling contact fatigue life of carburized AISI 8620 steel", *International Journal of Fatigue*, vol. 75, pp. 135-144, 2015. https://doi.org/ 10.1016/j.ijfatigue.2015.02.017.

[9] A. Aditya, F. S. Walvekar, Rolling contact fatigue of case carburized steels," *International Journal of Fatigue*, vol. 95, pp. 264-281, 2017. DOI:10.1016/j.ijfatigue.2016.11.003.

[10] H. Farivar, D. N. kshanov, S. D. L. Richter, W. Bleck, U. Prahl, "Core microstructure-dependent bending fatigue behavior and crack growth of a case-hardened steel", *Journal Materials Science and Engineering*, vol. 762, no. 5, pp. 1-24 , 2019. https://doi.org/ 10.1016/j.msea.2019.138040.

[11] Q. Yanfei, W. Bo, L. Shudan, Xiqiang, Ren., Z. Jingyi, L. Yungang, M. Jinjun, "Improved quantitative analysis method for evaluating fatigue cracks in thermal fatigue testing", *Journal Materials Letters*, vol. 242, pp. 115-118, 2019. https://doi.org/10.1016/j.matlet.2019.01.113.

[12] T. Zhenjie, W. Haoran, B. Christian, , S. Peter, "A unified fatigue life calculation based on intrinsic thermal dissipation and microplasticity evolution", *International Journal of Fatigue*, vol. 131, pp. 1-8, 2020. https://doi.org/ 10.1016/j.ijfatigue.2019.105370.

[13] W. Yanhui, , Z. Fucheng, B. L. Yang, Z. Chunlei, "Rolling contact fatigue performances of carburized and high-c nanostructured bainitic steels", *Journal of Materials*, vol. 9, no. 12, pp. 1-12 , 2016. https://doi.org/10.3390/ma9120960.

[14] K. Kohei, M. Tsuyoshi, U. Kohsaku, "Influence of Engaged Austenite on Sub-surface Initiated Spalling during Rolling Contact Fatigue in

Carburized SAE4320 Steel", *International journal of Transactions of the Iron and Steel institute of Japan*, vol. 60, no. 8, pp. 1774-1783, 2020. https://doi.org/10.2355/isijinternational.ISIJINT-2019-715.

[15] L.T. Sandor, I. Politori, C. S. Gonçalves, A. Y. C.V. Uehara, M. S. Leal, I. Ferreira, "Fatigue crack propagation in nine steels, type SAE 43XX, from 0.20 to 1.00 % C, for the simulation of the fatigue behavior in a carburized layer of the SAE 4320", *Journal Procedia Engineering*, vol. 2, no. 1, pp. 735-742, 2010. https://doi.org/10.1016/j.proeng.2010.03.079.

[16] Li Zhichao, M. Andrew, B. D. Freborg, T. S. S. Hansen, "Modeling the Influence of Carburization and Quenching on the Development of Residual Stresses and Bending Fatigue Resistance of Steel Gears", *Journal of Materials Engineering and Performance*, vol. 22, pp. 664-672, 2013. https://doi.org/10.1007/s11665-012-0306-0.

[17] L. Zhichao, "Heat treatment response of steel fatigue sample during vacuum carburization and high-pressure gas quenching process", *ASME 2015 International Manufacturing Science and Engineering Conference*, pp. 1- 6, 2015. https://doi.org/10.1115/MSEC2015-9395.

[18] I. Roslinda, A. Shahrum, T. Prakash, Z. O. Mohd, "An Experimental Investigation of Tensile Properties and Fatigue Crack Growth Behaviour for Dual Phase Steel", *Journal of Mechanical Engineering* , vol 15, no. 2, pp. 155-167, 2018.

[19] D. Hai Long, Bing, Liu, G. Yang, P. G. Yu, Huan, Yu., "Influence of local equivalent stress on fatigue life prediction of carburized Cr-Ni alloy steel based on evaluation of maximum crack sizes," *Journal of. Engineering Fracture Mechanics*, vol. 248, pp. 1-18, 2021, DOI: 10.1016/j.engfracmech.2021.107718.

[20] W. Mattias, M. Arne, "Influence of material, heat treatment, grinding and shot peening on contact fatigue life of carburized steels", *International Journal of Fatigue*, vol. 21, no. 4, pp. 309-327, 1999. https://doi.org/10.1016/S0142-1123(98)00077-2,

[21] R. S. Hyde, K. George, K. M. David, "The Influence of Reheat Treatments on Fatigue and Crack of Carburized Steels", *Journal of materials & manufacturing*, SAE Transactions, vol. 103, no. 5, pp. 588-596, 1994. https://doi.org/10.4271/940788.

[22] Z. Y. Zhao, R. G. Guan, Y. F. Shen, P. K. Bai, "Grain refinement mechanism of Mg-3Sn-1Mn-1La alloy during accumulative hot rolling. Journal of Mater", *Science Technology*, vol. 91, pp. 251–261, 2021. https://doi.org/10.1016/j.jmst.2021.02.052.

[23] C. H. Yin, Y. L. Liang, Y. Liang, W. Li, M. Yang, "Formation of a self-lubricating layer by oxidation and solid-state amorphization of nano-lamellar microstructures during dry sliding wear tests", *Journal of Acta Mater*, vol. 166, pp. 208–220, 2019. https://doi.org/10.1016/j.actamat.2018.12.049.

[24] Y. G. Cao, C. H. Yin, Y. L. Liang, S. H. Tang, "Lowering the coefficient of martensite steel by forming a self-lubricating layer in dry sliding wear, *Journal of Materials Research Express*, vol. 2019, no. 6, pp. 1-15, 2019. https://doi.org/10.1088/2053-1591/ab032a.

[25] Z. X. Li, B. Q. Tong, Q. L. Zhang, J. H. Yao, V. Kovalenko, "Microstructure refinement and properties of 1.0C-1.5Cr steel in a duplex treatment combining double quenching and laser surface quenching", *Journal of Material Science Engineering*, vol. 776, p. 138994, 2020. https://doi.org/10.1016/j.msea.2020.138994.

[26] J. N. Sultan, E. T. Karash, M. T. E. Kassim, A. M. Ali, H. A. Ibrhim, "The Effect of Carburization and Repeated Heat Treatment with Different Solutions on the Fatigue Resistance of Medium Carbon Steel", *International Journal of Heat and Technology*, vol. 40, no. 6, pp. 1478-1484, 2022. https://doi.org/10.18280/ijht.400616.

[27] J. N. Sultan, E. T. Karash, M. K. Najim, "Fatigue behaviour of tempered and isothermal heat treated AISI 5160 leaf spring steel", *Jurnal Teknologithis* , vol. 85, no. 3, pp. 15-24, 2023. Doi.org/10.11113/jurnalteknologi.v85.18640

[28] Z. X. Li, C.S. Li, J.Y. Ren, B.Z. Li, J. Zhang, Y.Q. Ma, "Effect of cold deformation on the microstructure and impact toughness during the austenitizing process of 1.0C–1.5Cr bearing steel", *Materials Science Engineering*, vol. 674, pp. 262-269. 2016. https://doi.org/10.1016/j.msea.2016.07.105.

[29] F. Wang, D. S. Qian, L. Hua, X. H. Lu, "The effect of prior cold rolling on the carbide dissolution, precipitation and dry wear behaviors of M50 bearing steel", *Tribology International Journal*, vol. 132, pp. 253-264, 2019. https://doi.org/10.1016/j.triboint.2018.12.031.

[30] J. N. Sultan, E. T. Karash, T. K. Abdulrazzaq, M. T. Elias Kassim, "The Effect of Multi-Walled Carbon Nanotubes Additives on the Tribological Properties of Austempered AISI 4340 Steel", *Journal Europeen des Systemes Automatises*, vol. 55, no. 3, pp. 387-396, 2022. https://doi.org/10.18280/jesa.550311

[31] G. Zhou, W. Wei, Q. Liu, , "Effect of Hot Rolling on Microstructural Evolution and Wear Behaviors of G20CrNi2MoA Bearing Steel", *Journal of Metals*, vol. 11, pp. 1-14, 2021. https://doi.org/10.3390/met11060957.

[32] H. Tada, P. Paris, G. R. Irwin, "The Stress analysis of cracks handbook", St. Louis, Paris Production Inc., 2nd Edition, 1985. https://doi.org/10.1115/1.801535

[33] J. P. Benthem, W. T. Koiter, "Asymptotic approximations to crack problems. In: Methods of analysis and solutions of crack problems", *Mechanics of fracture book series*, vol. 1, 1973. https://doi.org/10.1007/978-94-017-2260-5_3.